9-16-2022

Robotic Manufacturing System for Unattended Machining and Inspection of Graphite Bipolar Flow Field Plates for Proton Exchange Membrane Fuel Cells

Vladimir Gurau

Ryan Kent

Available online at www.sciencedirect.com

Manufacturing Letters

Manufacturing Letters 33 (2022) 56–65

50th SME North American Manufacturing Research Conference (NAMRC 50, 2022)

Robotic Manufacturing System for Unattended Machining and Inspection of Graphite Bipolar Flow Field Plates for Proton Exchange Membrane Fuel Cells

Vladimir Gurau* and Ryan Kent

Department of Manufacturing Engineering, Georgia Southern University, Statesboro, GA 30458, USA

*Corresponding author. Tel.: 912-478-5205. *E-mail address:* vgurau@georgiasouthern.edu

Abstract

A single robot-based manufacturing system for unattended machining and inspection of graphite bipolar flow field plates for proton exchange membrane fuel cells is designed and integrated for demonstration and validation. Unlike most robotic manufacturing systems where an industrial robot is used for tending an automated tool such as a computer numerical control machine, in the present system the industrial robot performs all manufacturing operations, including machining the flow fields on both sides of the plates, changing the tools, handling the plates, vacuuming the plates and the workholding device of graphite dust, flipping the plates, air blowing them and performing machine vision inspection for quality control. The toolpath for robotic machining the flow fields and the manifolds are generated offline using Roboguide simulation software. The manufacturing system uses an integrated machine vision inspection process as a diagnostic tool for in-line checking the presence of machined features and in-line verification of feature dimensions. Besides the considerably lower capital cost compared to other automated manufacturing systems resulted from the elimination of the automated machine tool, the proposed robotic cell has the advantage of better managing the abrasive graphite dust resulted in the manufacturing process. The limitations of the proposed robotic cell are assessed and recommendations for further development are considered. The manufacturing system is demonstrated as part of a larger endeavour of bringing to readiness advanced manufacturing technologies for renewable energy devices and responds the high priority needs identified by the U.S. Department of Energy for fuel cells manufacturing research and development.

Keywords: Robotic manufacturing system; unattended manufacturing and inspection; robotic manufacturing of PEMFCs

1. Introduction

Fuel cells directly convert the chemical energy in hydrogen to electricity, with pure water and useful heat being the only byproducts [1]. Fuel cells offer a broad range of benefits including efficient energy conversion, reduced greenhouse gas emissions, reduced air pollution, reduced oil consumption and highly reliable grid support. They also have significant advantages that make them attractive for end users, including quiet operation, low maintenance needs and high reliability. Compared to other types of fuel cells, the proton exchange membrane fuel cell (PEMFC), also known as polymer electrolyte membrane fuel cell, has the advantages of delivering higher volumetric and gravimetric power density and of operating at lower temperatures, which results in a quick start up time and less wear on systems components. For these reasons, PEMFCs currently find extensive applications in transportation and stationary uses.

A PEMFC stack consists of several unit cells connected in series and clamped together between two end plates. A unit cell consists of a membrane electrode assembly (MEA) placed between two electrically conductive bipolar plates that have flow field channels fabricated into both planar surfaces. An MEA consists of five components: a proton conductive membrane bounded by two catalyst layers, one on each side of the membrane, and two porous gas diffusion layers bonded each on the other side of the catalyst layers. Each unit cell is equipped with two gaskets placed on the peripheral area of each flow field which are intended to prevent reactant gas leaks or leaks between electrodes.

Nomenclature

D	tool diameter (inch)
DOC	depth of cut, (mm)
f_m	feed rate, (mm/min)
F_{fN}	Normal feed force on the cutting tool
f_t	feed per tooth, (mm/tooth)
L	length of cut (mm)
n	number of teeth, or flutes of the tool
RPM	rotations per minute
T_m	cutting time (min)
TCP	tool center point
EOA	end of arm
V	cutting speed, (m/min)

The bipolar flow field plates are key components of the PEMFC stack, accounting for 30% of the stack cost [2]. Their functions in the fuel cell are to connect the cells electrically, to house the flow fields and uniformly distribute the reactant and oxidant gasses over the active area of the cells, to separate and prevent the reactant and oxidant gasses in adjacent cells from mixing with each other, to conduct and distribute the heat produced during the electrochemical reaction and to provide structural support to the cells. Bipolar plates must have good electrical and thermal conductivity, good mechanical characteristics, low gas permeability, good chemical stability, must be lightweight, easily formable, and inexpensive. To meet these requirements, bipolar plates have been traditionally made from non-porous graphite, coated or non-coated metals or from graphite-based composite materials that include a polymer as binder and reinforcing agent [2-7].

PEMFC research and development (R&D) activities are oriented today towards achieving higher efficiency and durability along with identifying low materials and manufacturing costs [8]. Recent PEMFC published research focused on identifying new component materials [9-20], novel designs [21-27], new manufacturing methods [28-37], improved balance of plant [38-41] and on developing theoretical models and experimental diagnostics [42-53] that improve our understanding of fuel cells operation. Along with fundamental research, manufacturing R&D is needed to prepare advanced manufacturing and assembly technologies that are necessary for low-cost, high volume fuel cell powerplant production. U.S. Department of Energy (DOE) has identified high-priority manufacturing R&D needs for fuel cells [54]. A summary of these needs includes: (1) to develop technologies for high-speed manufacturing of fuel cell components; (2) to identify the cost of fuel cells at several levels of manufacturing; (3) to develop agile, flexible manufacturing and assembly processes; (4) to develop automated processes for assembling fuel cell stacks and (5) to establish flexible automated manufacturing technology facilities.

Two specific challenges identified by DOE [8] in manufacturing of fuel cells represent the lack of high-speed manufacturing processes for fuel cell bipolar plates and the quality control inspection necessary during manufacturing of fuel cell components.

Traditional fabrication processes for bipolar plates include processes for the formation of the base plates and processes for the formation of the flow field channels and manifolds [2-7]. Both processes can be integrated in a single manufacturing process using stamping of metal sheets or various compression techniques that include compression moulding and injection moulding of graphite-based composites. However, the highly abrasive nature of the graphite powder severely limits the life of the expensive moulds used for the fabrication of bipolar plates. To considerably lower the tooling cost, an alternative fabrication process represents the traditional milling of the flow fields in the base plate using computer numerical control (CNC) technology. Machining of graphite prohibits the use of cooling liquids but requires vacuuming the graphite dust produced during manufacturing. The abrasive graphite dust may severely damage the gear used for the actuation the CNC machine. An automated manufacturing system for high-volume, low-cost production of graphite bipolar plates would therefore consist of a CNC milling machine tended by an industrial robot for loading / unloading the plates and for vacuuming the graphite dust after machining each side of the plates.

Current inspection techniques used in the fuel cells industry often require off-line measurements, manual inspection techniques, and even destructive tests. These approaches slow the manufacturing process and add cost. The ramp-up to high-volume production of fuel cells requires in-line quality control and measurement technologies consistent with high-volume manufacturing processes [8].

This paper presents the design and demonstration of a robotic manufacturing system consisting of a single industrial robot (Fanuc LR Mate 200iD) used for unattended machining and inspection of graphite flow field plates for PEMFCs. The proposed robotic system is designed for high-volume, low-cost manufacturing and for improving the uniformity and repeatability of fabrication by increasing the automation level. Unlike most robotic manufacturing systems where an industrial robot is used for tending an automated machine tool, in the present system the industrial robot performs all manufacturing operations, including machining the flow fields on both sides of the plates, changing the tools, handling the plates, vacuuming the plates and the workholding device of graphite dust, flipping the plates, air blowing them and performing machine vision inspection for quality control. Besides the reduction of more than 50% in capital cost compared to other automated manufacturing systems resulted from eliminating the automated machine tool, the proposed robotic cell has the advantage of better managing the abrasive graphite dust resulted in the manufacturing process. To reduce the cycle time of the manufacturing process and ramp-up to high-volume production, the manufacturing system uses an integrated machine vision inspection process (Fanuc iRVision 2D) as a diagnostic tool for in-line checking the presence of machined features and in-line verification of feature dimensions.

Reviews of previous robotic machining application can be found in Chen and Dong [55], Iglesias et al. [56], Yuan et al. [57], or Ji and Wang [58]. The reviews conclude that in terms of accuracy, the industrial robot is worse than conventional machine tools. The main limiting factor to robotic machining is the low robot stiffness compared to CNC machines when the material hardness increases. Despite being a softer material, graphite is one of the most difficult materials to be machined [59-62]. Graphite can cause serious challenges as it can wear the tool and severely minimizes its life. When cutting graphite, the tool wear is caused by the abrasive nature of the graphite structure rather than by the cutting speed or material temperature. When the tool wears, the feed force and the radial force generated on the tool during the cutting process may become excessive, and in combination with the low robot stiffness may affect the dimensional accuracy of the machined features. The only effective way to machine graphite is using diamond coated tools which last 10-20 times longer than carbide tools [59-62].

The robotic manufacturing system presented in this paper was integrated to demonstrate the unattended fabrication and inspection of graphite bipolar plates for PEMFCs. It was also intended to acquire information regarding the optimum cutting parameters for further process optimization and minimization of the operation cycle. To our knowledge, this system represents the first attempt to fully automate the manufacturing of bipolar plates for fuel cells. The manufacturing system is demonstrated as part of a larger endeavour at Georgia Southern University of bringing to readiness advanced manufacturing technologies for renewable energy devices and responds the high priority needs identified by the U.S. Department of Energy for fuel cells manufacturing research and development.

2. Manufacturing System

The robotic cell was integrated to demonstrate the unattended fabrication and inspection of the graphite bipolar plate flow fields shown in Figure 1. The graphite plates (FuelCellStore.com) are 13 cm by 13 cm by 0.48 cm. The flow fields to be machined cover 100 cm^2 active area. The anode flow field consists of five 1/16”-wide and 0.05”-deep serpentine channels extending from an inlet manifold to an outlet manifold. The cathode flow field consists of 16 - 1/8”-wide and 0.08”-deep straight channels open to the atmosphere (air breathing fuel cell). The plates also have two ¼” diameter alignment holes and 8 – 8 mm diameter fastening holes.

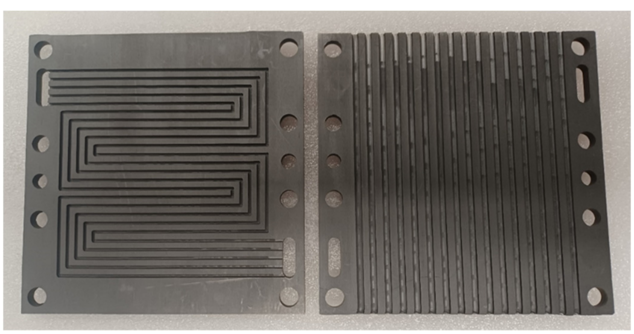

Fig. 1. Anode (left) and cathode (right) flow fields

The manufacturing system (Figure 2) consists of a Fanuc LR Mate 200iD industrial robot with R-30iB robot controller and Fanuc iRVision machine vision system mounted on a mobile cart having a 119 cm x 109 cm worksurface and equipped with air compressor, a TSS tool stand (ATI Industrial Automation) with four tools for automated tool changing, a fixed air blow nozzle, an in-house made pneumatic workholding device and fixtures for manufacturing operations, in-house integrated pneumatic and electronic controls, a fixed Sony XC-56 camera for in-line vision inspection and a Dayton dust collector for vacuuming the graphite dust. To minimize the spread of graphite dust during machining, the cart was placed with the workholding device near the intake of a MXT1500-100 ceiling-mounted fume extractor arm (Movex, Inc.). The robot end-of-arm (EOA) is equipped with a pneumatic QC11 master quick connect (ATI Industrial Automation) used to load / unload the tools required for the manufacturing operations. The quick connect is programmatically actuated by a robot factory mount solenoid valve through two complementary robot outputs (RO1 and RO2).

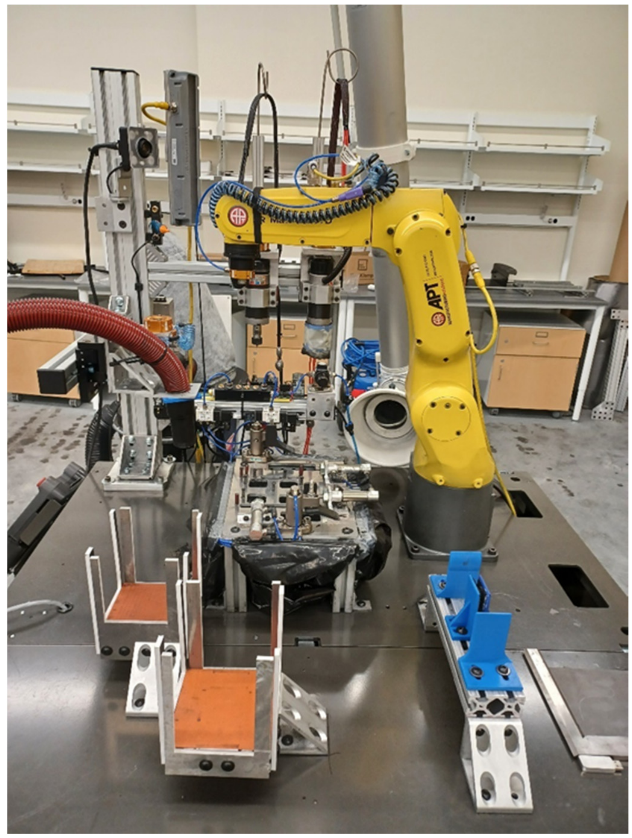

Fig. 2. Robotic system for unattended fabrication of fuel cell graphite flow field plates. The picture shows the TSS tool stand (ATI Industrial Automation) with four tools resting on it (far and left side), Sony XC-56 camera and lighting mounted on the tool stand (top-far-left), workholing device (center), two fixtures for picking up blank plates and stacking finished plates (front-left), fixture for flipping over the plates (front-right) and ceiling-mounted fume extractor arm (far-right)

2.1. Tooling

Four tools required for the manufacturing operations rest on the robot tool stand from where they are programmatically loaded / unloaded by the robot on its EOA before and after each operation. They are: (1) an in-house fabricated pneumatic gripper (Figure 3a) for handling the graphite plates, (2) an off-the-shelf 48 VDC, 20,000 RPM spindle with 1/16” end mill (Figure 3b) for machining the anode flow-field and the manifold holes, (3) an off-the-shelf 48 VDC, 20,000 RPM spindle with 1/8” end mill for machining the cathode flow-field (Figure 3c), and (4) a vacuum nozzle (Figure 3d) attached through a flexible hose to the dust collector for vacuuming the plates and the workholding device after each machining operation.

The pneumatic gripper (Figure 3a) consists of a ¼“-thick aluminium plate cut in-house using CNC waterjet on which four SLSA-120NR level compensators with suspension mechanisms and 10 mm vacuum cups (Anver Corporation) are mounted. The level compensators are used to provide a soft touch and to reduce machine indexing when picking up and releasing the graphite plates. The four vacuum cups are pneumatically connected through tubing and fittings mounted on the level compensators to a JV09CET miniature vacuum pump (Anver Corporation). The vacuum pump is connected to a robot factory-mounted solenoid valve actuated programmatically through two complementary robot outputs (RO3 and RO4). The aluminium plate is attached to a QC11 tool-side quick connect (ATI Industrial Automation) used to connect the tool to the robot EOA and a tooling interface plate (ATI Industrial Automation) used to attach the gripper to the tool stand when not in use.

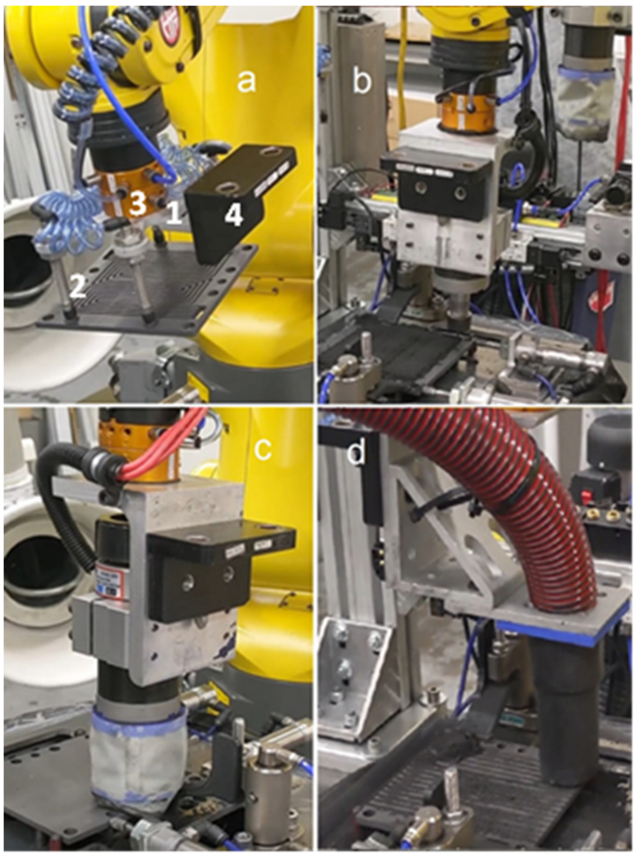

Fig. 3. Tooling: (a) Pneumatic gripper shown while handling a graphite plate with machined anode flow field; the numbers indicate: (1) - ¼"-thick aluminium plate; (2) - level compensators with suspension mechanisms; (3) - tool-side quick connect; (4) - tooling interface plate; (b) spindle with 1/16" end mill shown while machining the anode flow field and manifold holes; (c) spindle with 1/8" end mill and latex skirt shown while machining the cathode flow field; (d) vacuum nozzle loaded to the EOA shown while vacuuming of the cathode flow field.

The 48 VDC, 20,000 RPM spindles (Figures 3b an 3c) are attached to aluminium angle plates. QC11 tool-side quick connects (ATI Industrial Automation) used to connect the spindles to the robot EOA and tooling interface plates (ATI Industrial Automation) used to attach the spindles to the tool stand when not in use are also mounted to the angle plates. The spindle for machining the anode flow field and the holes (Figure 3b) is loaded with a 1/16"-diameter solid carbide square end mill. The spindle for machining the cathode flow field (Figure 3c) is loaded with a 1/8"-diameter solid carbide square end mill. To minimize the spread of graphite dust resulted in the machining process, this spindle has a 0.02"-thick latex skirt attached around the end mill. The spindles are programmatically turned on/off by the robot controller through digital outputs (DO105 and DO106 respectively).

The vacuum nozzle (Figure 3d) is attached to an aluminium U-shape profile reinforced with an 80/20 angle gusset used to minimize its vibrations while resting on the tool stand. The U-shape profile is attached to a QC11 tool-side quick connect (ATI Industrial Automation) used to connect the nozzle to the robot EOA and a tooling interface plate (ATI Industrial Automation) used to attach the nozzle to the tool stand when not in use. The nozzle is connected through a flexible hose to a Dayton dust collector. The dust collector is programmatically turned on/off by the robot controller through a digital output (DO107) that actuates a 24 VDC relay.

The fifth tool is a fixed air nozzle attached to the tool stand and is used to blow air and clean the plates after each machining operation. The air nozzle (Figure 4a) is pneumatically connected to the air compressor through a 3-way, 2-position Nitra BVS-32C2-24D solenoid valve (Automation Direct) which is programmatically actuated by the robot controller through a digital output (DO108).

The fixed Sony XC-56 camera and the LC-300 lighting system (Smart Vision Lights) are attached to the tool stand (Figure 4b). The camera is triggered programmatically by the vision system and the light is turned on/off programmatically by a robot output (RO8).

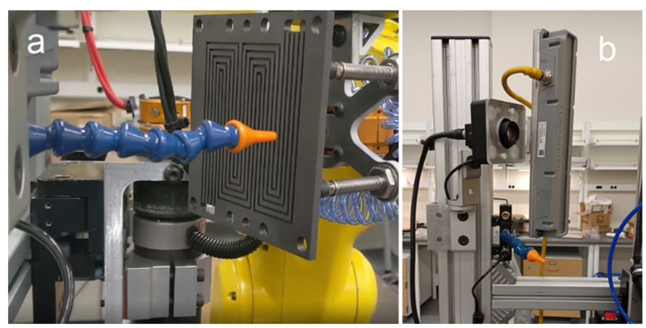

Fig. 4. (a) Fixed air nozzle shown while blowing air on the anode flow field. The plate is held by the robot gripper and moved relative to the nozzle; (b) fixed camera (Sony XC-56) and lighting system used for vision inspection

2.2. Fixtures

The automated workholding devise (Figure 5) used for locating and clamping the plates during machining was fabricated in house and consists of a ¼"-thick aluminium plate cut using CNC waterjet and having openings for collecting the graphite dust, 15 threaded, adjustable locators and supports, two AMWSW16 pneumatic swing clamps (IMAO Fixtureworks) used for vertical clamping and three double-action ¾"-bore air cylinders used for horizontal clamping the plates. The two vertical clamps and the three horizontal clamps are each connected pneumatically in cascade and actuated by two 4-way, 2-position Nitra AVS-5121-24D solenoid valves (Automation Direct) connected to the air compressor. A Nitra AR-223 pressure regulator is used to reduce the working pressure in the lines to 50 PSI. The vertical and horizontal clamps are programmatically turned on/off by the solenoid valves controlled by the robot controller through complementary pairs of digital outputs (DO101-DO102 and DO103-DO104, respectively). The workholding device is attached to the worksurface of the robot cart by four supports.

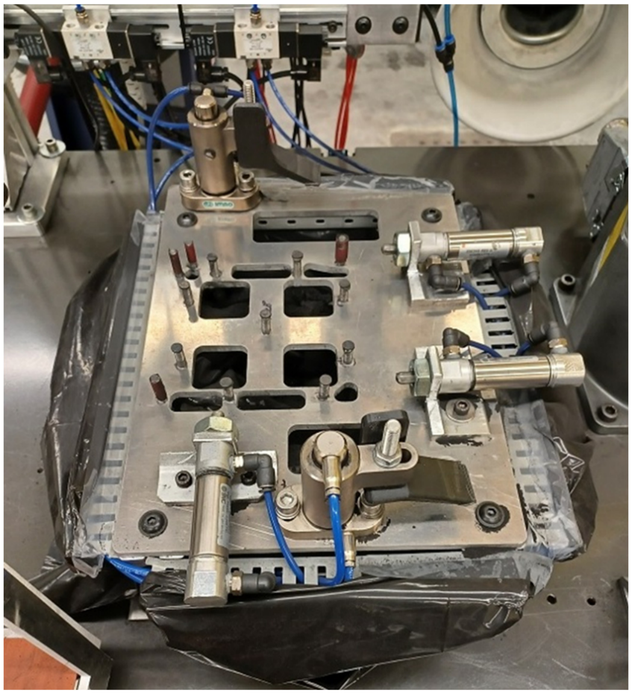

Fig. 5. Workholding device. The solenoid valves that actuate the vertical and horizontal clamps are visible in the far-left side of the picture.

A plastic bag is attached under the workholding device, between the supports to collect graphite dust.

Two fixtures from where the blank plates are picked (Figure 6a) and where the machined plates are stacked (Figure 6b), were fabricated in house using CNC waterjet. A fourth fixture (Figures 6c and 6d) is used by the robot to flip the plates from one side to the other. It has been fabricated in house using 3D printed parts attached to an 80/20 linear profile.

2.3. Robot programming

Today, complex robot toolpaths for machining operations can be generated using offline programming software. One method is to use a computer aided manufacturing (CAM) software such as Mastercam to generate the optimum cutting parameters and the toolpath for a CNC machine, then use a second software, such as Octopuz to convert the CNC toolpath to robot toolpath and generate the robot motion instructions. In this case, the cutting parameters such as depth of cut and feed rate are translated to the robot motion instructions. A second method is to use a robot simulation software having a computer aided manufacturing (CAD)–to–toolpath conversion feature. The 3D models of the part to be machined and of the tool to be used are imported in the virtual workspace of the robot and placed at their locations relative to the robot. The simulation program generates the toolpath and the robot motion instructions. This second method does not calculate the optimum cutting parameters.

For this demonstration, the toolpath for machining operations was generated using the Fanuc's Roboguide offline simulation software with its CAD-to-Path feature (Figure 7). To follow the practice adopted when machining graphite bipolar plates with CNC machines and increase productivity, the channels and holes were set to be cut in a single pass using end mills having the diameters equal to the channel widths. The cutting feed rate was set arbitrarily to 10 mm/s and the rapid

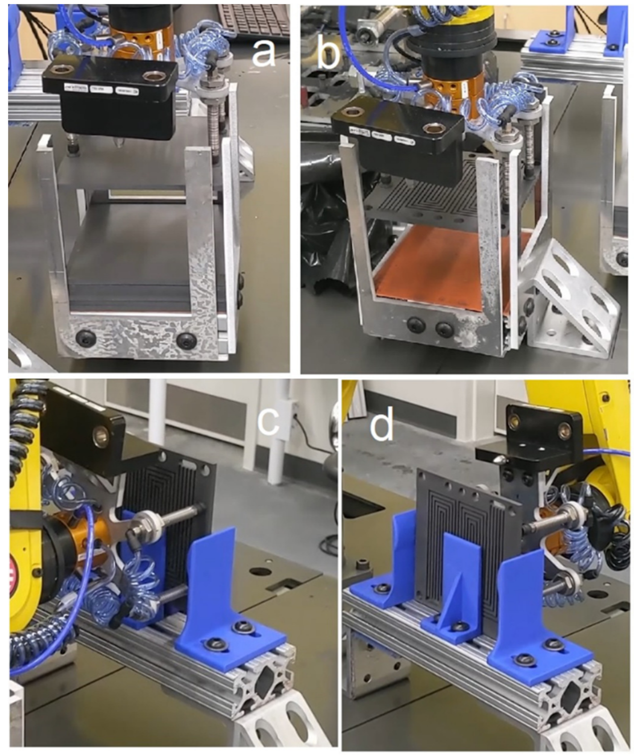

Fig. 6. Fixtures used in the robotic system. (a) fixture for blank plates shown while the robot picks a plate; (b) fixture for stacking machined plates shown while the robot places a plate. (c-d) fixture for flipping the plates. The robot flips a plate by placing it in the fixture while holding it from one side (c) and picking it from the other side (d)

moves between cuts to 100 mm/s. The robot motion instructions for machining operations ware uploaded as subroutines to the robot controller and the optimum cutting feed rate was determined experimentally by overwriting the motion speed using the OVERRIDE command of the Fanuc programming language.

All other subroutines for non-machining operations were created in leadthrough programming using the robot's teach pendant. The flowchart for the robotic operation cycle is shown in Figure 8. Each block in the flowchart corresponds to a robot subroutine.

The subroutines shown in Figure 8 are called from a main program. Based on the thickness of the plates and the number of machined plates, the program indexes the vertical position where blank plates are picked from and where the machined plates are placed to.

The vision inspection tasks were programmed offline using Fanuc's iRVision 2D software and a computer connected to the robot controller through ethernet IP protocol. Programs for three single view inspection vision processes were created for the anode side and one program was created for the cathode side to check the presence/absence of features and to evaluate critical features of the flow fields. The vision processes were taught based on a machined graphite plate used as reference. The vision processes are executed from the main program and based on judgement criteria passes or fails the process. Typical vision inspection results are shown in Figure 9.

The current setup does not identify malfunctioning or anomalous situations. The system may be improved by adding vision inspection tasks with multiple cameras, in which the presence or absence of the graphite plate in each fixture is monitored during machining and work handling operations.

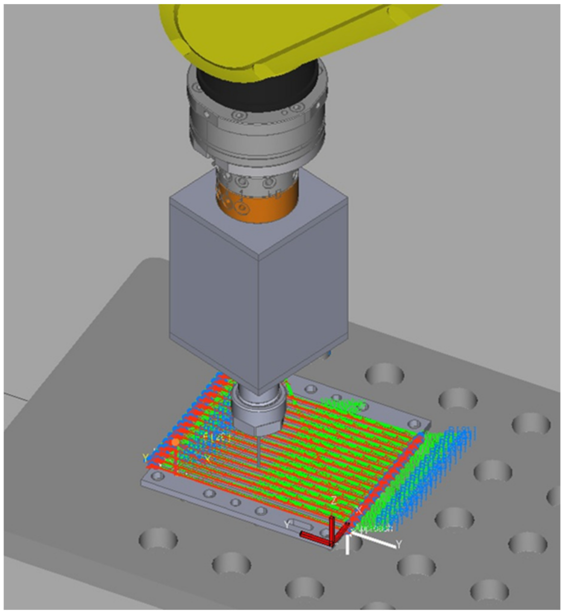

Fig. 7. Toolpath generated for the cathode flow field using Fanuc's Roboguide software

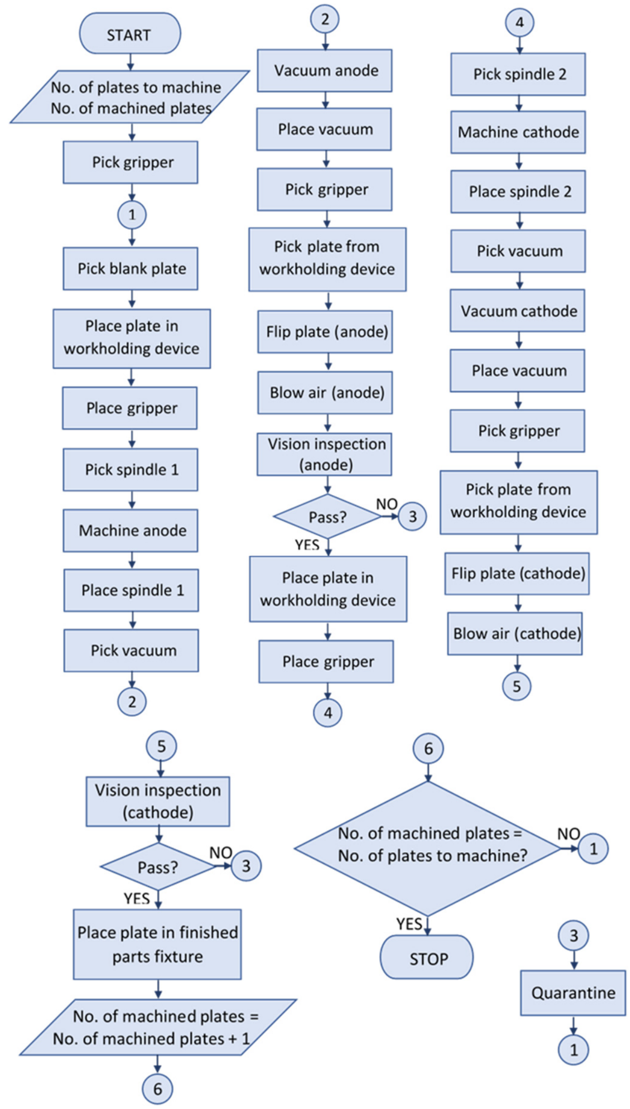

Fig. 8. Flowchart for robotic operation cycle

Table 1. Cutting parameters used in the demonstration.

Features	Tool	Depth of cut, *DOC* (mm)	Feed rate, f_m (mm/min)	Feed/tooth, f_t (mm/tooth)	Cutting speed, *V* (m/min)	Recommended feed/tooth and cutting speed, f_t/ *V* (mm/tooth)/(m/min) [60]
Holes and manifolds	1/16" DIA, 4-flute	4.8	60	0.00075	99,7	0.025-0.050/60-3,000
Anode flow field	1/16" DIA, 4-flute	1.3	150	0.0019	99,7	0.025-0.050/60-3,000
Cathode flow field	1/8" DIA, 4-flute	2.0	150	0.0019	1994	0.015-0.025/60-6,000

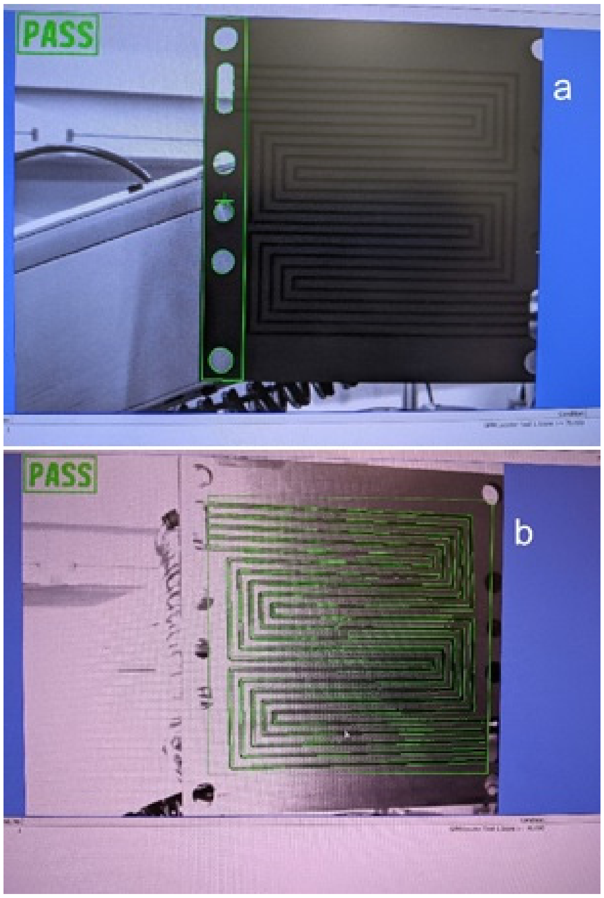

Fig. 9. Typical results of machine vision inspection used to check the presence/absence of features and to evaluate critical features of the flow fields; (a) inspection of holes and manifolds; (b) inspection of anode flow field

3. Results and Discussion

3.1. Optimum cutting parameters

The Roboguide simulation software used to generate the toolpath for machining operations does not calculate the optimum cutting parameters. The optimum feed rate was determined experimentally while the spindle RPM was maintained at its 20,000 RPM maximum value. All features were cut in a single path. The depth of cuts for each operation are shown in Table 1. The original 10 mm/s programmed feed rate (speed of tool centre point, TCP) resulted in severe deviations of the TCP from the programmed toolpath due to the low robot stiffness. Typical machine errors resulted when the feed rates were too high are shown in Figure 10.

The feed rates were reduced using the OVERRIDE command of the Fanuc's programming language until good dimensional accuracy was obtained. The optimum feed rates for each cutting operation are shown in Table 1. Table 1 also shows the calculated feed per tooth, cutting speed and recommended cutting parameters for graphite machining.

The feed per tooth, f_t (mm/tooth) and cutting speed, *V* (m/min) in Table 1 are calculated as [63]:

$$f_t = \frac{f_m}{n \times RPM} \quad (1)$$

$$V = 0.0254 \times RPM \times \pi \times D \quad (2)$$

The results indicate that the cutting speed and RPM used in the demonstration were within the recommended values for machining graphite, while the feed per tooth was one to two orders of magnitude lower. This is the result of keeping a low feed rate, f_m (speed of robot TCP) to prevent tool deviation from the programmed path when a robot with reduced stiffness is used. The cutting time, T_m of a milling process is calculated as [63]:

$$T_m = \frac{L}{f_m} \quad (3)$$

This equation along with the experimental results shown above indicate that to reduce the machining operation time and compete with CNC machining, robots with stiffer joints must be used. Alternative solutions to increase the productivity while keeping good dimensional accuracy and compete with CNC machining is to use spindles with increased RPM capabilities and/or cutting tools with increased number of flutes. Indeed, eq. (1) indicates that it is possible to proportionally increase the feed rate, f_m (speed of robot TCP) while keeping the same feed per tooth, f_t when increasing the spindle RPM and/or the number of tool flutes, *n*. Another technical solution to increase the productivity while keeping good dimensional accuracy is to adopt compliance error compensation techniques.

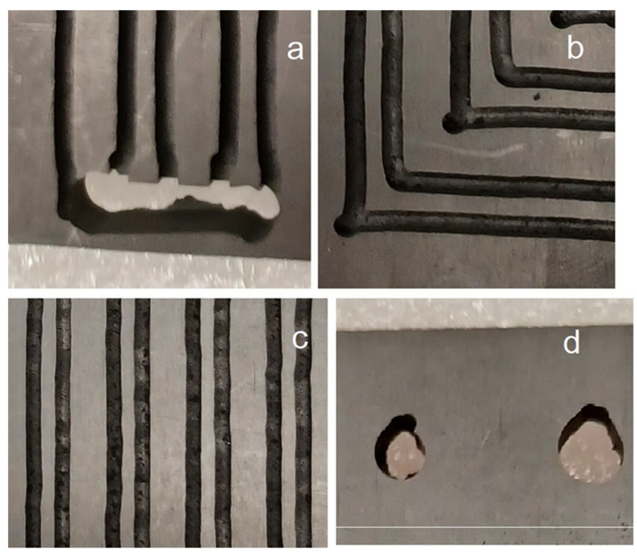

Fig. 10. Typical machining defects resulted from using large feed rates and a robot with low stiffness: (a) deviation of the toolpath at the start and end of the trajectory; (b) deviation of the toolpath when the direction of the trajectory changes; (c) unequally spaced channels. Note that in this image any two adjacent channels are cut in opposite directions; (d) excessive runout to circularity of holes.

The time for each operation is shown in Table 2. The operations in Table 2 correspond to the subroutines in Fig.8.

A video clip of the entire operation cycle is available at [64]. The operation cycle time can be improved mainly by reducing the time required for machining the anode and the cathode flow fields, which can be achieved by increasing the machining feed rate, f_m and using a robot with stiffer joints, spindles with higher RPM capabilities, tools with higher number of flutes, or by adopting compliance error compensation techniques.

Table 2. Operation time.

Subroutine	No. of times called	Operation time (s)	Total time (s)
Pick gripper	3	6	18
Pick blank plate from stack	1	21	21
Place plate in workholding device	2	6	12
Place gripper	2	8	16
Pick spindle 1	1	7	7
Machine holes and anode	1	1830	1830
Place spindle 1	1	7	7
Pick vacuum	2	8	16
Vacuum anode	1	52	52
Place vacuum	2	7	14
Pick plate from workholding device	2	9	18
Flip plate (anode)	1	27	27
Air blow anode	1	32	32
Vision inspection anode	1	7	7
Pick spindle 2	1	7	7
Machine cathode	1	904	904
Place Spindle 2	1	7	7
Vacuum cathode	1	87	87
Flip plate (cathode)	1	25	25
Air blow cathode	1	29	29
Vision inspection cathode	1	5	5
Place plate in finished parts fixture	1	28	28
Total operation cycle time (min)			52.82 min

3.2. Effect of tool wear on dimensional accuracy

When cutting graphite, the tool wear is caused by the abrasive nature of the graphite structure rather than by the cutting speed or material temperature. The only effective way to machine graphite is using diamond coated tools which last 10-20 times longer than carbide tools [59-62].

For this demonstration, the end mills used for the cutting operations were made of solid carbide. This resulted in a rapid tool wear that affected in time the dimensional accuracy of the flow field channels. When the tool wears, the normal feed force, F_{fN} which is generated on the tool during the cutting process and which is perpendicular to the tool trajectory becomes excessive, and in combination with the low robot stiffness affects the dimensional accuracy of the machined features. Figure 11 shows a first (left) and a fourth (right) anode flow field machined with the same tool. The highlighted channel segments are cut in opposite directions. The figure shows that the TCP was deviated from the programmed toolpath in a direction perpendicular to the tool trajectory. Table 3 shows the deviation from the programmed toolpath measured for the adjacent channels shown in Figure 11, for four plates machined consecutively using the same tool. To prevent this, diamond coated tools must be used.

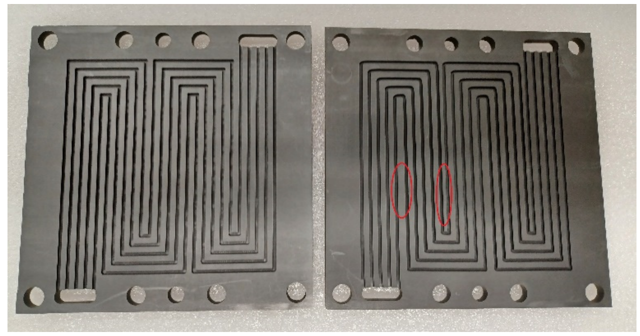

Fig. 11. Anode flow fields machined with the same end mill: the first plate (left) and the fourth plate (right). The figure shows that as the tool wears, the TCP deviates from the programmed toolpath in a direction perpendicular to the tool trajectory.

Table 3. Toolpath deviation due to tool wear, measured for four plates cut consecutively using with the same tool.

Plate	Deviation (mm)
First plate	0 ÷ 0.05
Second plate	0.09 ÷ 0.20
Third plate	0.31 ÷ 0.33
Fourth plate	0.39 ÷ 0.48

4. Conclusions

A single robot-based manufacturing system for unattended machining and inspection of graphite bipolar flow field plates for proton exchange membrane fuel cells (PEMFCs) was designed and integrated for demonstration and validation. Unlike most robotic manufacturing systems where an industrial robot is used for tending an automated tool such as a CNC machine, in the present system the industrial robot performs all manufacturing operations, including machining the flow fields on both sides of the plates, changing the tools, handling the plates, vacuuming the plates and the workholding device of graphite dust, flipping the plates, air blowing them and performing machine vision inspection for quality control.

The toolpath for robotic machining the flow fields were generated offline using Roboguide simulation software with its CAD-to-Path feature. The manufacturing system uses an integrated machine vision inspection process (Fanuc iRVision 2D) as a diagnostic tool for in-line checking the presence of machined features and in-line verification of feature dimensions.

Besides the considerably lower capital cost compared to other automated manufacturing systems resulted from the elimination of the automated machine tool, the demonstrated robotic cell has the advantage of better managing the abrasive graphite dust resulted in the manufacturing process.

To prevent toolpath deviation from the programmed trajectory due to reduced robot stiffness, the feed rates used in the cutting operations were one-to-two orders of magnitude lower than the ones recommended for machining graphite. To reduce the machining operation time and compete with CNC machining, one must use robots with stiffer joints, spindles with higher RPM capabilities, tools with higher number of flutes, or by adopting compliance error compensation techniques.

Acknowledgements

This work was made possible with funds from Georgia Southern University.

References:

[1] U.S. Department of Energy: Hydrogen Fuel Cells. Available from: https://www.nrc.gov/docs/ML1002/ML100280723.pdf (accessed on November 28, 2021)

[2] Taherian, R. A Review of Composite and Metallic Bipolar Plates in Proton Exchange Membrane Fuel Cell: Materials, Fabrication, and Material Selection. *J. Power Sources* **2014**, 265, 370-390. DOI:10.1016/j.jpowsour.2014.04.081

[3] Mehta, V.; Cooper, J.S. Review and Analysis of PEM Fuel Cell Design and Manufacturing, *Journal of Power Sources* **2003**, 114, 32-53. DOI:10.1016/S0378-7753(02)00542-6

[4] Tsuchiya, H.; Kobayashi, O. Mass Production Cost of PEM Fuel Cell by Learning Curve. *Int. J. Hydrogen Energy* **2004**, 29, 985-990. DOI:10.1016/j.ijhydene.2003.10.011

[5] Suherman, H.; Sahari, J.; Sulong, A.B. Effect of Small-Sized Conductive Filler on the Properties of an Epoxy Composite for a Bipolar Plate in a PEMFC. *Ceramics International* **2013**, 39, 7159-7166. DOI:10.1016/j.ceramint.2013.02.059

[6] Muller, A.; Kauranen, P.; von Ganski, A.; Hell, B. Injection Moulding of Graphite Composite Bipolar Plates. *J. Power Sources* **2006**, 154, 467–471. DOI:10.1016/j.jpowsour.2005.10.096

[7] Yeetsorn, R.; Fowler, M.W.; Tzoganakis, C. A Review of Thermoplastic Composites for Bipolar Plate Materials in PEM Fuel Cells. In *Nanocomposites with Unique Properties and Applications in Medicine and Industry*; Editor Cuppoletti J. Publisher: InTech, London, 2011, pp. 317-344 ISBN 978-953-307-351-4. DOI: 10.5772/19262

[8] Hydrogen and Fuel Cell Technologies Office: Chapter 3.5. Manufacturing R&D, in *Multi-Year Research, Development, and Demonstration Plan*. **2015**. Available from: https://www.energy.gov/sites/default/files/2015/06/f22/fcto_myrdd_manufacturing.pdf (accessed on November 28, 2021)

[9] Roth, C.; Bleith, P.; Schwoebel, C.A.; Kaserer, S.; Eicher, J. Importance of Fuel Cell Tests for Stability Assessment—Suitability of Titanium Diboride as an Alternative Support Material. *Energies* **2014**, 7, 3642–3652.

[10] Hwang, K.; Kim, J.H.; Kim, S.Y.; Byun, H. Preparation of Polybenzimidazole-Based Membranes and Their Potential Applications in the Fuel Cell System. *Energies* **2014**, 7, 1721–1732.

[11] Liu, J.; Yuan, Y.; Bashir, S. Functionalization of Aligned Carbon Nanotubes to Enhance the Performance of Fuel Cell. *Energies* **2013**, 6, 6476–6486.

[12] Stassi, A.; Gatto, I.; Sacca, A.; Baglio, V.; Arico, A.S. Enhancement of Oxygen Reduction and Mitigation of Ionomer Dry-Out Using Insoluble Heteropoly Acids in Intermediate Temperature Polymer-Electrolyte Membrane Fuel Cells. *Energies* **2015**, 8, 7805–7817.

[13] Balzarotti, R.; Latorrata, S.; Stampino, P.G.; Cristiani, C.; Dotelli, G. Development and Characterization of Non-Conventional Micro-Porous Layers for PEM Fuel Cells. *Energies* **2015**, 8, 7070–7083.

[14] Kiatkittkul, P.; Nohira, T.; Hagiwara, R. Nonhumidified Fuel Cells Using N-Ethyl-N-methyl-pyrrolidinium Fluorohydrogenate Ionic Liquid-poly (Vinylidene Fluoride-Hexafluoropropylene) Composite Membranes. *Energies* **2015**, 8, 6202–6214.

[15] Endo, N.; Ogawa, Y.; Ukai, K.; Kakihana, Y.; Higa, M. DMFC Performance of Polymer Electrolyte Membranes Prepared from a Graft-Copolymer Consisting of a Polysulfone Main Chain and Styrene Sulfonic Acid Side Chains. *Energies* **2016**, 9, 658.

[16] Sgambetterra, M.; Brutti, S.; Allodi, V.; Mariotto, G.; Panero, S.; Navarra, M.A. Critical Filler Concentration in Sulfated Titania-Added Nafion Membranes for Fuel Cell Applications. *Energies* **2016**, 9, 272.

[17] Jang, H.; Sutradhar, S.C.; Yoo, J.; Ha, J.; Pyo, J.; Lee, C.; Ryu, T.; Kim,W. Synthesis and Characterization of Sulfonated Poly (Phenylene) Containing a Non-Planar Structure and Dibenzoyl Groups. *Energies* **2016**, 9, 115.

[18] Wang, C.; Wang, S.; Peng, L.; Zhang, J.; Shao, Z.; Huang, J.; Sun, C.; Ouyang, M.; He, X. Recent Progress on the Key Materials and Components for Proton Exchange Membrane Fuel Cells in Vehicle Applications. *Energies* **2016**, 9, 603.

[19] Latoratta, S.; Stampino, P.G.; Cristiani, C.; Dotelli, G. Performance Evaluation and Durability Enhancement of FEP-Based Gas Diffusion Media for PEM Fuel Cells. *Energies* **2017**, 10, 2063.

[20] Gurau, V.; Zawodzinski, T.; Wayne, R. In-situ Characterization of GRAFCELL® Flexible Graphite Film as Gas Diffusion Layers for PEMFCs, *ECS Transactions* **2008**, 16, 1651-1659. DOI: 10.1149/1.2982006

[21] Ma, H.; Cheng,W.; Fung, F.; Hsu, C.; Lin, C. Compact Design of 10 kW Proton Exchange Membrane Fuel Cell Stack Systems with Microcontroller Units. *Energies* **2014**, 7, 2498–2514.

[22] Chen, Y.S.; Lin, S.M.; Hong, B.S. Experimental Study on a Passive Fuel Cell/Battery Hybrid Power System. *Energies* **2013**, 6, 6413–6422.

[23] Jeong, S.K.; Lee, J.S.;Woo, S.H.; Seo, J.A.; Min, B.R. Characterization of Anion Exchange Membrane Containing Epoxy Ring and C–Cl Bond Quaternized by Various Amine Groups for Application in Fuel Cells. *Energies* **2015**, 8, 7084–7099.

[24] Cheng, S.; Xu, L.; Li, J.; Fang, C.; Hu, J.; Ouyang, M. Development of a PEM Fuel Cell City Bus with a Hierarchical Control System. *Energies* **2016**, 9, 417.

[25] Byun, S.J.; Wang, Z.H.; Son, J.; Kwak, D.K.; Kwon, Y.C. Experimental Study on Improvement of Performance by Wave Form Cathode Channels in a PEM Fuel Cell. *Energies* **2018**, 11, 319.

[26] Bozzini, B.; Bocchetta, P.; Gianocelli, A. Coelectrodeposition of Ternary Mn-Oxide/Polypyrrole Composites for ORR Electrocatalysts: A Study Based on Micro-X-ray Absorption Spectroscopy and X-ray Fluorescence Mapping. *Energies* **2015**, 8, 8145–8164.

[27] Gurau, V.; Zawodzinski, C.; Zawodzinski, T.; Wainright, J. Fuel Cell System with Flow Field Capable of Removing Liquid Water from the High-Pressure Channels, US Patent 8,029,942. 2011.

[28] Gurau, V.; Fowler, D.; Cox, D. Robotic Technologies for Proton Exchange Membrane Fuel Cell Assembly. In *Proton Exchange Membrane Fuel Cells*; Editor Taner T. Publisher: InTech, London, 2018, pp. 21-34. ISBN: 978-1-78923-066-6. DOI: 10.5772/intechopen.69180

[29] Fowler, D.; Gurau, V.; Cox, D. Bridging the Gap between Automated Manufacturing of Fuel Cell Components and Robotic Assembly of Fuel Cell Stacks, *Energies*, **2019**, 12, 3604. DOI:10.3390/en12193604

[30] Gurau, V.; Cox, D.; Fowler, D.; Carter, M.; Ogunleke, A. Design and Demonstration of Automated Technologies for the Fabrication and Testing of PEM Fuel Cell Systems, *International Journal of Mechanical Engineering and Robotics Research*. **2020**, 9, 640. DOI: 10.18178/ijmerr.9.5.640-645

[31] Gurau, V.; Armstrong-Koch, T. Further Improvements of an End-Effector for Robotic Assembly of Polymer Electrolyte Membrane Fuel Cells, *Energies*, **2015**, 8, 9452. DOI: 10.3390/en8099452

[32] Williams, M.; Tignor, K.; Sigler, L.; Rajagopal, C.; Gurau, V; Robotic Arm for Automated Assembly of Proton Exchange Membrane Fuel Cell Stacks, *J. Fuel Cell Sci. Technol.*, **2014**, 11, 054501-1. DOI: 10.1115/1.4027392

[33] Laskovski, C.; Derby, S; Fuel Cell ASAP: Two Iterations of an Automated Stack Assembly Process and Ramifications for Fuel Cell Design-For-Manufacture, *J. Fuel Cell Sci. Technol.*, **2011**, 8, 031004-1. DOI: 10.1115/1.4000684

[34] KUKARobotGroup. The Production of Proton Exchange Membrane Fuel Cells with a KUKA Robot. Available online: https://www.youtube.com/watch?v=E-vcRR4mC6w (accessed on November 28, 2021)

[35] Konold, P.; Muminovic, A.; and Wehreim, M. Assembly of Fuel Cells and Stacks with Robots. In *Research and Education in Robotics: EUROBOT 2008*, Gottscheber A. et al., Eds., Springer-Verlag, 2009, 168. DOI:10.1007/978-3-642-03558-6

[36] Zentrum für BrennstoffzellenTechnik. Fuel Cell Manufacturing Plant/Automatisierte Brennstoffzellenmontage am ZBT. Available online: https://www.youtube.com/watch?v=KhrcHO_qw80 (accessed on November 28, 2021)

[37] Gurau, V. Robotic Fuel Cell Assembly System, US Patent 2015/0158179 A1, 2015

[38] Lee, H.S.; Cho, C.W.; Seo, J.H.; Lee, M.Y. Cooling Performance Characteristics of the Stack Thermal Management System for Fuel Cell Electric Vehicles under Actual Driving Conditions. *Energies* **2016**, 9, 320.

[39] Qin, Y.; Wang, X.; Chen, R.; Shangguan, X. Water Transport and Removal in PEMFC Gas Flow Channel with Various Water Droplet Locations and Channel Surface Wettability. *Energies* **2018**, 11, 880.

[40] Gurau, V.; Ogunleke, A.; Strickland, F. Design of a Methanol Reformer for On-Board Production of Hydrogen as Fuel for a 3kW High-Temperature Proton Exchange Membrane Fuel Cell Power System, *International Journal of Hydrogen Energy* **2020**, 45, 31745; DOI:10.1016/j.ijhydene.2020.08.179

[41] Han, J.; Charpentier, J.F.; Tang, T. An Energy Management System of a Fuel Cell/Battery Hybrid Boat. *Energies* **2014**, 7, 2799–2820.

[42] Gurau, V.; Castro, E.D.: Prediction of Performance Variation Caused by Manufacturing Tolerances and Defects in Gas Diffusion Electrodes of Phosphoric Acid (PA)–Doped Polybenzimidazole (PBI)-Based High-Temperature Proton Exchange Membrane Fuel Cells, *Energies* **2020**, 13, 1-14; DOI:10.3390/en13061345

[43] San Martin, I.; Ursua, A.; Sanchis, P. Modelling of PEM Fuel Cell Performance: Steady-State and Dynamic Experimental Validation. *Energies* **2014**, 7, 670–700.

[44] Chang, L.Y.; Chen, H.C. Linearization and Input-Output Decoupling for Nonlinear Control of Proton Exchange Membrane Fuel Cells. *Energies* **2014**, 7, 591–606.

[45] Kulikovsky, A. Polarization Curve of a Non-Uniformly Aged PEM Fuel Cell. *Energies* **2014**, 7, 351–364.

[46] Tavcar, G.; Katrasnik, T. An Innovative Hybrid 3D Analytic-Numerical Approach for System Level Modelling of PEM Fuel Cells. *Energies* **2013**, 6, 5426–5485.

[47] Alink, R.; Gerteisen, D. Modeling the Liquid Water Transport in the Gas Diffusion Layer for Polymer Electrolyte Membrane Fuel Cells Using a Water Path Network. *Energies* **2013**, 6, 4508–4530

[48] Gurau, V.; Mann, J.A.; Zawodzinski, T.A. Numerical Investigation of Water Transport in the PEMFC Components, *ECS Transactions* **2006**, 3, 1095-1104. DOI: 10.1149/1.2356229

[49] Vinh, N.D.; Kim, H.M. Comparison of Numerical and Experimental Studies for Flow-Field Optimization Based on Under-Rib Convection in Polymer Electrolyte Membrane Fuel Cells. *Energies* **2016**, 9, 844.

[50] Choi, J.S.; Sohn, J.Y.; Shin, J. A Comparative Study on EB-Radiation Deterioration of Nafion Membrane in Water and Isopropanol Solvents. *Energies* **2015**, 8, 5370–5380.

[51] Gurau, V. Response to "Comment on 'A Look at the Multiphase Mixture Model for PEM Fuel Cell Simulations'" *Electrochem. Solid-State Lett.* **2009**, 12, S4-S6. DOI: 10.1149/1.3041657

[52] Mao, L.; Davies, B.; Jackson, L. Application of the Sensor Selection Approach in Polymer Electrolyte Membrane Fuel Cell Prognostics and Health Management. *Energies* **2017**, 10, 1511.

[53] Gurau, V.; Mann, J.R. Technique for Characterization of the Wettability Properties of Gas Diffusion Media for Proton Exchange Membrane Fuel Cells. *Journal of Colloid and Interface Science* **2010**, 350, 557. DOI: 10.1016/j.jcis.2010.07.011

[54] U.S. Department of Energy: Roadmap on Manufacturing R&D for the Hydrogen Economy. Available from: https://www.hydrogen.energy.gov/pdfs/roadmap_manufacturing_hydrogen_economy.pdf (accessed on November 28, 2021)

[55] Chen, Y.; Dong, F. Robot Machining: Recent Development and Future Research Issues. *Int. J. Adv. Manuf. Technol.* **2013**, 66, 1489–1497. DOI:10.1007/s00170-012-4433-4

[56] Iglesias, I.; Sebastián, M.A.; Ares, J.E. Overview of the State of Robotic Machining: Current Situation and Future Potential. *Procedia Engineering* **2015**, 132, 911–917. DOI: 10.1016/j.proeng.2015.12.577

[57] Yuan, L.; Pan, Z.; Ding, D.; Sun, S.; Li, W. A Review on Chatter in Robotic Machining Process Regarding both Regenerative and Mode Coupling Mechanism. *IEEE/ASME Trans. Mechatronics* **2018**, 23, 2240–2251. DOI:10.1109/TMECH.2018.2864652

[58] Ji, W.; Wang, L. Industrial Robotic Machining: a Review. *Int. J. Adv. Manuf. Technol.* **2019**, 103, 1239–1255. DOI:10.1007/s00170-019-03403-z

[59] Harvey Performance Company. Grappling with Graphite: A Machining Guide. Available from: https://www.harveyperformance.com/in-the-loupe/grappling-with-graphite/ (accessed on November 28, 2021)

[60] Decatur Diamond. Graphite Machining. Available from: https://decaturdiamond.com/documents/Graphite%20Machining.pdf (accessed on November 28, 2021)

[61] Yin, S.W. Graphite Milling, the Proper Way. Available from: https://www.edmsalesinc.com/wp-content/uploads/2014/06/Graphite_milling_the_proper_way.pdf (accessed on November 28, 2021)

[62] Kopeliovich, D. Machining Graphite and Carbon. Available from: https://www.substech.com/dokuwiki/doku.php?id=machining_graphite_and_carbon (accessed on November 28, 2021)

[63] Black, J.T.; Kohsher, R.A. Chapter 24: Milling. In *Degarmo's Materials and Processes in Manufacturing*; 11th Edition, Publisher: John Wiley & Sons, Inc., 2012, pp. 665-685. ISBN-13: 978-0-470-92467-9.

[64] Manufacturing Engineering, Georgia Southern University. Manufacturing Engineering Student Integrates Robot-based Flexible Manufacturing Cell for Unattended Machining and Inspection of Fuel Cell Flow Field Plates. Available from: https://cec.georgiasouthern.edu/manufacturing-engineering/2021/08/17/manufacturing-engineering-student-integrates-robot-based-flexible-manufacturing-cell-for-unattended-machining-and-inspection-of-fuel-cell-flow-field-plates/ (accessed on November 28, 2021)